Physica Medica 60 (2019) 58–65

Contents lists available at ScienceDirect

Physica Medica

journal homepage: www.elsevier.com/locate/ejmp

Original paper

Early survival prediction in non-small cell lung cancer from PET/CT images using an intra-tumor partitioning method

Mehdi Astaraki[a,b], Chunliang Wang[a,*], Giulia Buizza[c], Iuliana Toma-Dasu[b,d], Marta Lazzeroni[b,d], Örjan Smedby[a]

[a] KTH Royal Institute of Technology, Department of Biomedical Engineering and Health Systems, Hälsovägen 11C, SE-14157 Huddinge, Sweden
[b] Karolinska Institutet, Department of Oncology-Pathology, Karolinska Universitetssjukhuset, Solna, SE-17176 Stockholm, Sweden
[c] Politecnico di Milano, Department of Electronics, Information and Bioengineering, piazza Leonardo da Vinci 42, Milan 20133, Italy
[d] Stockholm University, Department of Physics, SE-10691 Stockholm, Sweden

ARTICLE INFO

Keywords:
Survival prediction
Treatment response
Radiomics
Tumor heterogeneity

ABSTRACT

Purpose: To explore prognostic and predictive values of a novel quantitative feature set describing intra-tumor heterogeneity in patients with lung cancer treated with concurrent and sequential chemoradiotherapy.
Methods: Longitudinal PET-CT images of 30 patients with non-small cell lung cancer were analysed. To describe tumor cell heterogeneity, the tumors were partitioned into one to ten concentric regions depending on their sizes, and, for each region, the change in average intensity between the two scans was calculated for PET and CT images separately to form the proposed feature set. To validate the prognostic value of the proposed method, radiomics analysis was performed and a combination of the proposed novel feature set and the classic radiomic features was evaluated. A feature selection algorithm was utilized to identify the optimal features, and a linear support vector machine was trained for the task of overall survival prediction in terms of area under the receiver operating characteristic curve (AUROC).
Results: The proposed novel feature set was found to be prognostic and even outperformed the radiomics approach with a significant difference ($AUROC_{SALoP}$ = 0.90 vs. $AUROC_{radiomic}$ = 0.71) when feature selection was not employed, whereas with feature selection, a combination of the novel feature set and radiomics led to the highest prognostic values.
Conclusion: A novel feature set designed for capturing intra-tumor heterogeneity was introduced. Judging by their prognostic power, the proposed features have a promising potential for early survival prediction.

1. Introduction

Lung cancer is one of the most frequently diagnosed cancers. It is a leading cause of cancer death with a global number of deaths of 1.69 million in 2015 [1,2]. The most frequent type of lung cancer (85% of all lung cancers) is Non-Small Cell Lung Cancer (NSCLC), which is often diagnosed in stage III and thus not suitable for surgical resection and, instead, specific chemoradiation therapy is prescribed [3,4].

Tumor response to treatment is traditionally assessed by using size-based criteria such as World Health Organizations (WHO) criteria or Response Evaluation Criteria in Solid Tumors (RECIST) [5]. In this type of analysis, measuring anatomical changes of the tumor size after completion of the whole cycle of therapy, tumor response is categorized in four main groups designated as complete response, partial response, stable and progression. Nevertheless, there exist cases in which the tumors may not shrink significantly despite effective treatment such as lymphoma, sarcoma, hepatomas, mesothelioma, and gastrointestinal stromal tumor [6,7]. In addition, some chemotherapy methods may yield tumor haemorrhage, necrosis, or cavitation which is not necessarily relevant to the tumor shrinkage. Accordingly, the changes in morphology, function or metabolic activity of a tumor after therapy cannot be presented accurately by using only size-based measurements [8]. Considering the limitations of anatomical response metrics, PET Response Criteria in Solid Tumors (PERCIST) have been proposed to allow quantitative assessments [9]. As a multimodal imaging, 18F-Fludeoxyglucose-PET-CT (FDG-PET-CT) is capable of quantitatively detecting tumor glucose metabolic change and hence, is used for treatment response assessment as early as the second week of chemoradiotherapy cycle. To do so, PET-CT images are being utilized for early assessment response by visual evaluations or measuring the

* Corresponding author at: Hälsovägen 11C, SE-14157 Huddinge, Sweden.
E-mail address: chunwan@kth.se (C. Wang).

https://doi.org/10.1016/j.ejmp.2019.03.024
Received 27 October 2018; Received in revised form 12 February 2019; Accepted 21 March 2019
Available online 27 March 2019

changes in Standard Uptake Value (SUV) [9,10]. However, parameters such as SUV_{max}, commonly used in this type of assessments, measure the maximum activity within an image voxel and do not take into account the variations in the distribution of FDG uptake within the whole tumor volume and, moreover, they are quite sensitive to image resolution and the level of noise [6].

Recently, numerous studies have focused on developing more advanced quantitative measurements of physiological features within the images to capture cancer imaging phenotypes which can reflect information related to the patho-physiological properties of the tumor [11–15]. By converting medical images into high-dimensional mineable data and by extracting a large number of quantitative features automatically/semi-automatically, radiomics offer new opportunities in decision support, personalized and precision medicine in the field of oncology [16–18]. However, it has been found that radiomic features are quite sensitive to factors such as scanner settings, organ motion, segmentation method and model overfitting [19,20]. In order to identify the radiomic features which are reproducible under the same acquisition parameters, dimensionality reduction after analysis of test–retest data sets has been investigated [4,5,11,19,21].

For NSCLC, radiomics have been employed for the tasks of early treatment assessment and overall survival as well as distant metastasis prediction [3,8,22]. Although using only CT-based features led to results lower than 0.84 in terms of area under the receiver operating characteristic curve (AUROC) and lower than 0.7 in terms of Concordance Index (CI) [3,22–24], it has been found that adding PET features may improve the prognostic results [6,25]. Recent studies have postulated and, to some extent, demonstrated, that partial tumor response to the therapy can be explained by the existence of sub-regions within the tumor volume with different sensitivities to treatment, giving rise to intra-tumor heterogeneity with respect to chemoradiosensitivity [8,26–28]. To address the challenge of quantifying the intra-tumor heterogeneity, a longitudinal feature set, Longitudinal Pattern (LoP), was recently proposed [29]. In that study it was hypothesized that the tumor physiology and microenvironment leading to the formation of sub-volumes with different vasculature and interstitial fluid pressure conditions can be characterised by dividing the tumor volume into a given number of separate zones based on the distance from the tumor boundaries. A major limitation of such a feature set is its arbitrary choice of the same number of zones regardless of the tumor size which would result in thin zones that hardly differ from each other in small tumors and thus are less well suited to represent differences within the tumor mass. Inspired by [29] we have, in this study, taken into account the fact that the tumor volume is different for the patients included in the analysed cohort and generally in a clinical cohort, unless intentionally selected based on the tumor volume. Thus, we introduced an extended version of LoP, Size-Aware Longitudinal Pattern (SALoP), and tested it as an imaging biomarker for survival prediction in NSCLC from PET-CT images after validation on a test-retest data set. Fig. 1 shows a graphical illustration of the overall study design.

2. Material and methods

2.1. Patient data

The data set includes 30 patients with 31 tumors, all diagnosed with NSCLC in stage III except three cases who were in stages I, II and IV. This parameter was then considered as a covariate as described in discussion section. The 15 patients in the sequential group underwent 3 cycles of cisplatin-gemcitabine before the beginning of Radiation Therapy (RT), whereas the other 15 patients, belonging to the concurrent group, received one cycle of cisplatin-vinorelbine before RT and 2 cycles during RT. The patients in the sequential group were irradiated with 2 fractions of 1.8 Gy per day, reaching either the tolerated normal tissue toxicity limit or the prescribed maximum dose of 79.2 Gy. On the other hand, a dose escalation protocol was chosen as a treatment plan for the patients in the concurrent group which included delivering of 30 fractions of 1.5 Gy twice per day as the first step and then 2 Gy fractions once per day until reaching either the limit of the normal tissue toxicity or the maximum prescribed dose of 69 Gy. A 3D conformal treatment plan was calculated based on the International Commission on Radiation Units and Measurements guidelines [30] and inhomogeneities were corrected by employing a fast Fourier transform convolution algorithm. Patients were irradiated with a linear accelerator (Elekta SL 15, Elekta Oncology Systems, United Kingdom or Siemens Oncor, Siemens Medical Solutions, CA). Treatment verification was performed using electronic portal imaging device measurements [31]. Patients were imaged with a Biograph 40 PET scanner (Siemens Medical Solution) to acquire one FDG-PET-CT scan before the beginning of radiation therapy and another one with the same scanner settings during the second week of radiotherapy. While planning was done using a 4D respiration-correlated CT, a primary 3D CT was used for this study. PET images were corrected for scatter and decay, rebinned and reconstructed using a 2D ordered-subset expectation maximization algorithm with 4 iterations and 8 subsets. Acquisition parameters were homogeneous across patients and the injected FDG activity was calculated as 4 times the body weight in Kg plus an additional of 20 MBq [32]. The most important clinical details of the patients can be found in Table 1 in Supplementary Material.

2.2. Image pre-processing

Prior to feature extraction, all images were pre-processed in two steps. First, intensity normalization was performed to bring the intensity levels to the same scale between the patients. PET intensities were converted into SUV units, whereas CT intensities were converted to Hounsfield units and then normalized by a linear transformation. Rescale slope and intercept parameters of the linear equation were calculated through averaging the voxel intensities inside two regions of interest of lung air and cardiac pool. In the second step, images were resampled to $0.98 \times 0.98 \times 0.98$mm using a bi-cubic interpolation function.

2.3. Tumor segmentation

The reproducibility of most of the extracted features depends to a great extent on the segmented regions. Although most radiomics studies have manually segmented the tumors, it has been shown that the results have high inter-observer variability [33]. Therefore, a fast and robust 3D level set segmentation method was utilized to semi-automatically delineate the gross tumor volume (GTV) [34,35]. An intensity-threshold-based energy functional, along with reinitialization-free coherent propagation, drive the initial contour toward the target boundaries. The availability of blocking tools in the software helped to prevent the evolving contour from leaking into nearby structures. The accuracy of the segmentation results has been investigated by an expert radiologist and manually refined. The segmentation process was performed on CT and PET images separately and also performed on the pre-treatment and second scans independently.

2.4. Image registration

Intra-subject image registration was performed in two steps by aligning the CT images from the second scans to the pre-treatment scans. First, manual CT image registration was applied on the whole lung region by visually defining the corresponding anatomical landmarks [36]. In the second step, automatic registration was restricted only to the region surrounding the tumor mask to force a more precise alignment in the tumor region [37]. Finally, PET-PET image registration was executed by applying the same transformations obtained from corresponding CT images to the PET images. It should be noted that the PET and CT images for each patient were intrinsically registered

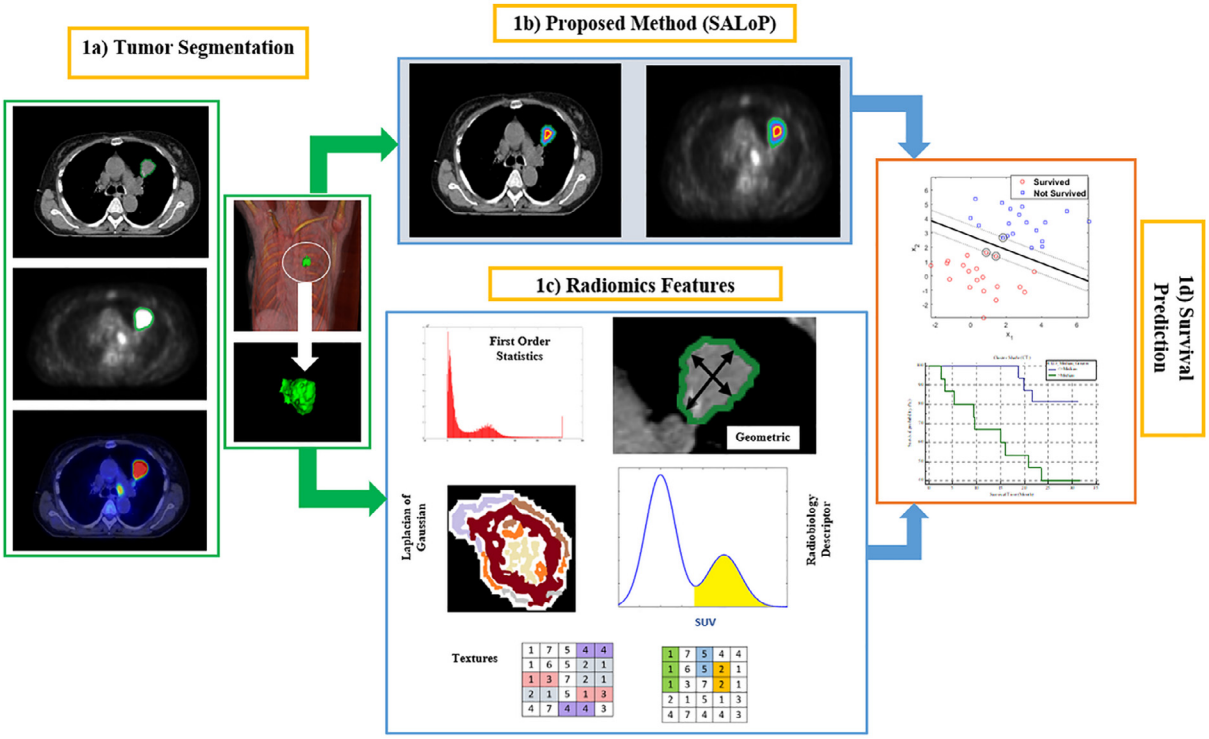

Fig. 1. Schematic illustration of the study pipeline. a) GTV was segmented in PET-CT images with a semi-automatic algorithm and 3D visualization of the tumor volume. b) Tumor volume was divided into different regions for extracting SALoP features. c) Radiomic features were extracted from the tumor volume. d) Features were analyzed to assess their prognostic values.

together during the acquisition with a hybrid PET-CT machine.

2.5. Size-Aware Longitudinal Pattern

Inspired by the feature set proposed in [29], we introduced a new feature set, Size-Aware Longitudinal Pattern (SALoP), which aims at quantifying the spatial and temporal variations in the structure and function of the tumor. In this study, the volume of pre-treatment GTVs varied from 3.21 to 236.11 cm^3. To capture the heterogeneity within the tumor, we hypothesized that the sensitivity of tumor cells to treatment varies as a function of the distance from the tumor borders, therefore by differentiating the tumor volume into separate regions, metabolic activity and characteristics of tumor cells may be identified from more homogeneous regions. Therefore, we partitioned the GTV into different sub-regions based on their distance to the tumor borders. To compute the SALoP, the Euclidean distance of each voxel inside the GTV from tumor borders was calculated and then divided by the maximum distance for normalization. These distances were then divided linearly into 1–10 groups, representing the partitioned regions.

The division process was done in such a way that for every 0.5 cm of distance from the tumor borders, one region was added. Hence, the smallest tumor, with a radius of 0.5 cm, was considered as only one region and the biggest tumor, with a 5 cm radius, was divided into ten regions counting outwards, so that the tumor core was set as the first partition and the regions adjacent to the tumor borders were assigned as the tenth partition, as illustrated in Fig. 2. Then, by calculating the average voxel intensity inside each sub-region, GTVs were converted into 1–10 quantitative features. To make all the feature vectors equal in size, a padding technique was employed, i.e., by repeating the average intensity inside the last partitioned region (for the cases with less than 10 sub-regions), every CT and PET image for each patient was transformed into a feature vector with a length of 10. The underlying hypothesis behind the padding technique is the fact that the normal tissue outside the tumor volume is homogeneous with respect to

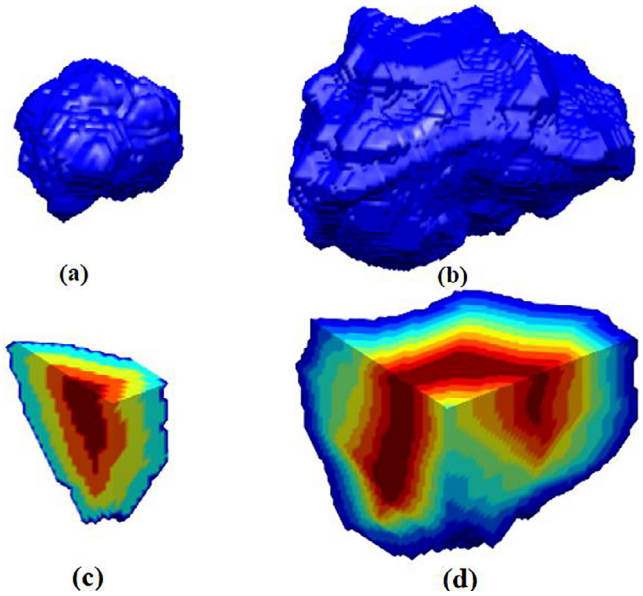

Fig. 2. 3D surface plot of a mid-size tumor (a) and the largest tumor in the data set (b). The lower row depicts two cross sectional iso-surfaces of the tumor masses that were partitioned into 5 and 10 separate sub-regions based on the distance of the sub-regions from tumor boundaries where each sub-region is represented by a different color. Cores of the tumors were considered as the first region and the outermost layer as the last region. Images were magnified and are not in real scale.

chemoradiosensitivity. Finally, the feature set for each patient was designed by subtracting the average intensity within one partition zone of the second scan from the corresponding one in the first scan (delta SALoP), for PET and CT images separately. Thus, each patient was

Table 1
Prognostic values of SALoP feature set, radiomics and their combination without forward feature selection. For each case, the highest value is marked in bold. AUROC values significantly different from 0.50 (randomness) are indicated with *.

Modality	Therapy	AUROC					
		10-Fold			Leave One Out		
		SALoP	Radiomics	SALoP + Radiomics	SALoP	Radiomics	SALoP + Radiomics
CT	Sequential	0.80*	0.73	**0.90***	0.87*	0.80	**0.92***
	Concurrent	**0.66**	0.51	0.51	**0.70**	0.49	0.50
	All	0.64	0.58	**0.66**	0.66	0.56	**0.69**
PET	Sequential	**0.86***	0.68	0.71	**0.85***	0.73	0.73
	Concurrent	**0.80**	0.61	0.63	**0.80***	0.63	0.65
	All	**0.87***	0.62	0.63	**0.86***	0.61	0.63
PET-CT	Sequential	**0.92***	0.68	0.69	**0.94***	0.78	0.76
	Concurrent	**0.84***	0.63	0.65	**0.83***	0.65	0.69
	All	**0.90***	0.63	0.69	**0.90***	0.71	0.66

represented by a feature vector with a length of 20. It should be noted that all the above-mentioned calculations were performed over the union masks which means that separate masks from the pre-treatment and second scans were merged together for each modality per patients, and the SALoP was extracted from the merged union mask.

Since the longitudinal data set used in this study were acquired from the same machine under similar acquisition parameters and radiotherapy position, the robustness of the proposed novel feature set with respect to the factors such as segmentation and processing method, as well as anatomical changes was investigated. Therefore, SALoP features were also extracted from RIDER test–retest data set [38–40] and their reproducibility was examined.

2.6. Radiomic features

To validate the performance of the SALoP feature set, a radiomic analysis was performed by extracting a total number of 451 3D descriptors from PET-CT images. Radiomic features were extracted by following the standard procedures recommended by the Image Biomarker Standardization Initiative (IBSI) [41]. In specific, second order statistics features were extracted after applying a Lloyd quantization method with a fixed number of 128 and 32 bins for PET and CT images, respectively. All the analyses were performed on PET and CT images with isotropic scales of 5 and 3 mm. PET images were prepared with a square root histogram transformation as suggested in [42]. Then, from each of PET and CT images 13 first-order statistics, 53 second-order statistics, 18 geometric and 130 multi-scale textural features were extracted separately by following the exact parameters and formulas as defined in [22] which agrees with [41]. Moreover, 3 SUVs ($SUV_{max,mean,peak}$) from PET images and 20 radio-sensitivity features as defined in [43] were added to the feature pools. More details over the mentioned features was presented in Table 2 in the Supplementary Material. A union mask was generated by merging the segmentation masks of the single-timepoint scans. The radiomic features, except for the geometric ones, were extracted from the union mask while geometric radiomics were calculated from the single-timepoint masks. Here, we applied the Concordance Correlation Coefficient (CCC) [44] on the RIDER test-retest data set to identify reproducible CT features. A CCC value of 0.80 was used as a threshold for reproducibility, i.e., CT radiomics with CCC $\geq$ 0.80 were considered as stable features. Then, two sets of features were built by extracting the radiomic features from pre-treatment scans (F_{pre}) and the second scans (F_{sec}). The final radiomic features were designed by computing the differences between the two sets, i.e. delta features, ($\Delta F = F_{sec} - F_{pre}$). In addition to perform the analysis over the delta features, radiomic features from the pre-treatment and second scans were analyzed separately and compared against the SALoP features from single-timepoint scans.

2.7. Feature selection and prediction model

Feature selection is a means to reduce the dimensionality of a large set of features and to remove irrelevant features with respect to target labels. In this study, feature selection was performed by using Forward Feature Selection (FFS) [45] as a wrapper algorithm. A Linear Support Vector Machine (LSVM) was employed as a classifier and prediction performance was assessed with AUROC [46,47]. The process of the FFS starts by feeding the features one by one to the LSVM and the feature with the highest prediction performance was kept. Then, the rest of the features were combined one after another to the retained feature and the same procedure continued until no improvement in prediction performance was observed. Because of the small size of input data, and to minimize the risk of overfitting, the classification process was evaluated through 10-fold and Leave-One-Out (LOO) cross-validations. Confidence intervals at the 95% level were employed to statistically test significant differences between the computed AUROC and random performance (AUROC = 0.50) [49]. FFS was performed 30 times for each feature set, and the most frequently repeated features with the highest prediction power resulted from the test data and false discovery rate [5,48] corrected p-values below 0.05 were retained as the most informative features. Finally, by feeding them to an LSVM, the prognostic power of the proposed feature set, radiomics and their combinations were examined (Tables 1 and 2). All implementations were made on a desktop computer in MATLAB 9.2 software (©Mathworks, Natick, MA) with an in-house developed toolbox and an open access radiomics toolbox [42,50]. To test the statistical significance in pairwise comparison of SALoP and radiomics ROC curves, the method proposed by Delong was utilized [51].

2.8. Clinical endpoints

All the patients were followed up for 2 years after the last session of RT. The endpoint for training the machine learning model was defined as the binary overall survival status after 2 years. Specifically, the outcome was set as positive if the patients were alive 2 years after the therapy and negative if the patients were deceased at that time-point. Length of the follow-up for each patient is presented in Table 1 in Supplementary Material.

2.9. Survival analysis

Features with AUC values above 0.6 in the FFS were included in a survival analysis, based on individual follow-up times, using Cox Proportional Hazard Regression. For each feature significantly contributing to the prediction, Kaplan–Meier curves were drawn, and a Log-rank test performed, for the subpopulations defined by a median

Table 2
Prognostic values of SALoP feature set, radiomics and their combination with forward feature selection. For each case, the highest value is marked in bold. AUROC values significantly different from 0.50 (randomness) are indicated with *.

Modality	Therapy	AUROC					
		10-Fold			Leave One Out		
		SALoP	Radiomics	SALoP + Radiomics	SALoP	Radiomics	SALoP + Radiomics
CT	Sequential	**0.93***	0.91	**0.93***	0.92*	0.76	**0.95***
	Concurrent	0.48	0.50	**0.53**	0.53	0.50	**0.70**
	All	0.68*	0.85*	**0.86***	0.71*	0.87*	**0.89***
PET	Sequential	0.91*	0.95	**0.98**	0.91*	0.97	**0.99**
	Concurrent	0.87*	**1***	**1***	0.90*	**1***	**1***
	All	0.88*	0.89*	**0.95***	0.89*	0.87*	**0.96***
PET-CT	Sequential	0.92*	0.95*	**0.98**	0.95*	0.96*	**0.98**
	Concurrent	0.93*	**1**	**1***	0.91*	**1**	**1***
	All	**0.94***	0.90*	**0.94***	**0.95***	0.86*	**0.95***

threshold [17].

3. Results

3.1. Reproducibility of Size-aware longitudinal pattern and CT radiomics

First of all, the reproducibility of the proposed feature set was substantiated by achieving a high agreement (CCC > 0.92) when the SALoP feature set was applied to the RIDER test-retest data set. In addition, by applying the test-retest analysis on radiomics, 47 percent of all CT radiomic features was identified as stable and reproducible features, and the remaining 53 percent was removed from the feature pools. The results are presented in Table 2 in Supplementary Material.

3.2. Size-aware longitudinal pattern and longitudinal pattern

Partitioning the tumor into separate sub-regions based on the tumor size contributed to a remarkable improvement in prognostic values in most of the experiments. In fact, without applying FFS, the overall survival prediction power in all the PET-CT images was improved from $AUROC_{LoP} = 0.85$ to $AUROC_{SALoP} = 0.90$. This improvement was also observed with the FFS method, where the survival prediction for all the PET-CT images was enhanced from $AUROC_{LoP} = 0.92$ to $AUROC_{SALoP} = 0.95$. Moreover, with FFS, prognostic values of SALoP outperformed LoP in concurrent therapy for PET and PET-CT images, and in sequential therapy for CT images. These improvements were observed with both the 10-fold and LOO cross-validation methods. On the other hand, the LoP method with FFS resulted in higher prediction values in sequential therapy for PET and PET-CT images and in concurrent therapy for CT images.

3.3. Size-aware longitudinal pattern, radiomics and their combination

Comparing the results between SALoP feature set and radiomics, one can observe that the novel proposed feature set outperformed the radiomics significantly when prediction was done without feature selection (Table 1). Dimensionality reduction with FFS in delta radiomics resulted in 12 features from PET, 15 features from CT, and 11 features from PET-CT images; however, only 2 features from PET, 3 from CT and 3 from PET-CT delta SALoP feature sets were selected. More details over the prognostic radiomics and the selected features for all the experiments can be found in Table 3 at Supplementary Material. Feeding the prediction model with selected features, radiomics performed slightly better than SALoP in most of the cases, whereas the combination of SALoP and radiomics rendered the highest values of prediction power (Table 2). The statistical significance in pairwise comparison of SALoP and radiomics ROC curves is given in Table 4 (Supplementary Material) in terms of p-values.

3.4. Size-aware longitudinal pattern and imaging modality

Comparing the PET images with CT images in terms of SALoP prediction values, it can be noted that PET-based features have higher prognostic values than CT-based features, both with and without FFS, except for the case of sequential therapy where prediction scores of CT features were slightly higher than PET features. In addition, the highest prediction scores of SALoP set were obtained by combining PET and CT features together. The same trend can be observed for the radiomic approach without FFS and with 10-fold cross validation FFS; however, no clear pattern was found in FFS along with the LOO algorithm. Surprisingly, the combined PET features of SALoP and radiomic, with FFS, not only outperformed combined CT features of SALoP and radiomic, but also resulted in a slightly higher prediction power than the corresponding PET-CT features.

3.5. Single-timepoint analysis

Tables 5 and 6 in Supplementary Material show the average AUROC values, along with their standard deviations, resulting from performing the whole experiments for the single-timepoint scans, i.e. SALoP and radiomic features from the pretreatment and second scans were analyzed separately. It should be noted that the performance of the model with the LOO method, when feature selection is not applied will result in exactly similar values, so that no variation can be observed (Supplementary Material, Table 5 LOO column). It can be seen that for all the SALoP, radiomics and their combinations, features extracted from the separate scans resulted in lower prediction values than the delta features, except the case of CT radiomics without FFS, where the pretreatment features outperformed the delta features.

In addition, compared to the radiobiological descriptors which were performed on 29 out of the 31 datasets (because of unavailability of all dose maps) [43], PET-CT SALoP features performed better, improving the prognostic values of sequential therapy from 0.81 to 0.95, whereas for the concurrent therapy radiobiological features resulted in higher prediction values 0.96 vs. 0.91.

3.6. Size-aware longitudinal pattern, radiomics and survival analysis

The overall parameters and coefficients of the fitted Cox regression model are presented in Tables 7 and 8 (Supplementary Material). The results indicated that the selected delta and pre-treatment features for both of the SALoP and radiomics were significantly related to survival time. While two delta SALoP features contributed significantly to the model prediction, only one feature was identified for single-timepoint

SALoP sets. Kaplan-Meier curves of the median-thresholded features (Figs. 1–3 Supplementary Material) show significant differences in survival for seven of the delta and single-timepoint features, both in the SALoP and the radiomics set.

4. Discussion

The main objective of this study has been to develop a new physiologically meaningful feature set that is capable of capturing intra-tumor heterogeneity based on the properties of CT and PET images. To this end, we partitioned each tumor into separate sub-regions and from each zone, mean intensity changes for PET and CT images respectively was utilized as a quantitative feature to describe physiological traits of distinct parts of the tumors, such as variations in metabolic activity and oxygenation, as well as tissue inflammation. Since remarkable intensity variation inside each of the sub-regions was not observed, we could infer that tumor properties were homologous in partitioned regions. In contrast, the LoP method [29] divided every tumor into 10 zones regardless of the tumor size; thus for tumors with small sizes, several separate regions would be produced with the same physiological properties that does not properly reflect distinct characteristics and therefore would not be able to accurately discriminate between heterogeneous regions.

Performing FFS on delta SALoP features, inner layers were identified as prognostic features in PET images while for CT images features combining inner and outer layers represented more prognostic values. Although this behavior was not exactly the same in single-timepoint scans, the combination of PET-CT SALoP resulted in a similar trend for all the delta and single-timepoint features, i.e., the second inner layer of CT, the third inner layer of PET as well as either the first or the second inner layers of PET images were selected as the most informative features. On the other hand, in delta LoP feature set, the most informative CT features were the first, third, and tenth layers, while only the third layer was identified for PET images. Therefore, although the selected features in SALoP and LoP were not exactly similar, they indicated the same behavior. In other words, in PET images the sub-regions closer to the tumor core and in CT images the combination of subregions closer to the core and tumor boundaries were most prognostic.

A contrary behaviour distinguished between SALoP and LoP methods on sequential and concurrent therapies with FFS. In fact, PET and PET-CT SALoP features from concurrent therapy outperformed the same ones from LoP, as the selected SALoP features from the concurrent therapy had the highest similarity with those observed for the combination of sequential and concurrent therapies. On the other hand, the selected PET and PET-CT LoP features from concurrent therapy were slightly inconsistent with the selected ones resulting from the combination of the two therapies. The same trend was also detected for selected CT features in sequential therapy. Accordingly, whenever the selected features from separate therapies complied with the ones from the combination of the two therapies, SALoP method outperformed LoP and vice versa.

Another advantage of the proposed method is the limited number of extracted features, i.e. each tumor volume was translated into 20 features or only about 4% of the size of radiomic features. Despite the small size of the SALoP feature set, prognostic values outperformed the radiomics results in all the cases when FFS was not applied. It can be seen that without FFS, the prediction power (AUROC) of radiomic features was in the range between 0.63 and 0.71 for all the PET-CT images, while the same values for the SALoP method lay around 0.90, i.e. a substantial improvement. This implies that each partition of the tumor has its own specific properties that are captured well by the proposed method and the combination of different partitions together represents the diversity inside the tumors effectively. Besides, by using FFS, the prediction results of SALoP features were still close to those of radiomics. Applying FFS resulted in an improvement of almost 27 percent (0.63–0.90) in prognostic power of radiomic features and 5 percent (0.90–0.95) for the proposed method (for PET-CT images with LOO cross validation). This means that large numbers of radiomic features were either redundant or lacking informative value, whereas the SALoP features hold a similar informative content. Accordingly, it can be inferred that partitioning a tumor volume into sub-regions based on the similarity of the distances to the tumor borders has a potential to reflect the tumor phenotypes regardless of whether feature selection was applied or not. Besides that, the improved prediction power resulting from the combination of SALoP and radiomics suggests that these features might be complementary. In fact, SALoP features reflect, to some extent, both geometric properties and first order statistics, which are two major radiomic feature families. Furthermore, adding PET features to the CT features may help to better capture early therapy response when the detectable anatomical changes in CT images are not evident, so that analyzing the metabolic changes in tumor region measured from PET images would be beneficial. This was observed in the SALoP feature set when the delta PET features combined with delta CTs in FFS yielded an improvement in prediction power. This result is also in agreement with other studies [6,52].

Analyzing the pre-treatment and second scans separately reveals the fact that for the SALoP features, either with or without FFS, the prediction power of the PET and PET-CT images was decreased in the second scan; however, CT-based features of the second scan were more prognostic. It can also be seen that pre-treatment scans have more prognostic values than the second scans in the combined SALoP and radiomic feature set. Compared to a recently proposed intra-tumor partitioning method [28], the prediction power of the pretreatment PET-CT SALoP outperformed a more complicated partitioning method (0.80 ± 0.15 vs. 0.75). Moreover, compared to delta features, it can be understood that investigating the single timepoint features yielded lower values of prediction scores with SALoP, radiomics and their combinations except the case of CT radiomics without FFS. This could be related to the LSVM model struggling in solving the problem with so many features that again highlights the importance of dimensionality reduction.

Applying the FFS along with cross-validation on radiomics and the combination of SALoP and radiomic features minimized the risk of overfitting problem. The selected radiomic features were consistent with the prognostic radiomics which were reported in other studies on NSCLC. In specific, 9 of the selected CT radiomics and 5 of the selected PET radiomics were reported by other authors as prognostic radiomic features [3,17,53–57]. In addition, almost half of the selected features were belong to textural radiomics which agreed with the findings by other studies that texture features hold high prognostic values for predicting tumor response to the therapy [53,58–61]. Although tumor volume was not selected as a prognostic feature from geometric radiomics neither for PET nor for CT images, it should be noted that SALoP feature set was designed based on the tumor volume as the number of the tumor sub-regions directly depends on the tumor size. Therefore, it cannot be excluded that tumor volume could still play an important role in the evaluation of tumor response to therapy. Furthermore, removing the unstable features that were identified from the test–retest analysis led to a remarkable improvement in the prediction values comparing to the result of the recent study on the same data set where stability test was not performed [29]; in fact, the AUROC values on PET-CT images increased from 0.60 (concurrent therapy) and 0.88 (sequential therapy) to 1 and 0.96 respectively. It also worth mentioning that extracting a large number of features from a relatively small data set without feature selection increases the risk of overtraining. However, removing almost 53 percent of non-reproducible CT radiomics from the feature pools, and performing the analyses with LOO and 10-fold cross validations after precisely investigating the training and validation losses, assured us that the reported results were not overfitted.

The high reproducibility suggests that the SALoP feature set has the potential to distinguish slight differences between different tumor

phenotypes so that the SALoP feature set may yield non-redundant and stable results. Moreover, the reproducible radiomic features identified in this study agreed with the results from other studies on the same test-retest dataset [5,11,19]. Thus, the utilized pre-processing steps as well as segmentation method seem to be reliable for imaging biomarker analysis purposes. It should also be noted that tumor stages were also added to the feature pools as an additional feature; however, it did not change the results neither with FFS nor without it. Finally, the overall prediction power achieved by the proposed feature set in this study is comparable to other studies [17,46,62], though they utilized different data sets.

It is noticeable that although the training of the machine learning model (LSVM) was based on survival at one single-timepoint (after two years), some of the selected features from LSVM, were then able to predict individual survival times. In fact, a SALoP signature with 2 features and radiomics signature with 4 features resulted in significant Cox Proportional Hazard Regression models. Although we used a relatively low threshold value (AUROC$\geq$ 0.6) for features to be included in the Cox model, the identified significant features were among the prognostic features resulted from LSVM. In specific, in the SALoP set, the layers closer to the tumor core, the second and third layers of PET and CT images, were significantly contributed to the model prediction. For delta SALoP, the features with the values lower than the median threshold and for the pre-treatment and second scan SALoP, features with values above the median resulted in higher survival rates. Moreover, the non-significant split of Kaplan-Meier curves over half of the identified significant features, could be related to the small size of the data set.

Although the achieved results of this study are encouraging, there still exist certain limitations. First, the proposed partitioning method is based only on tumor geometry, i.e., distance from the tumor border, and does not contain other tumor characteristics. Future work should therefore tackle this shortcoming by partitioning the tumor into sub-regions based on more sophisticated criteria such as advanced clustering or SUV variations and extracting the radiomic features from sub-regions instead of the whole tumor mass. Second, generalization of the proposed method would further strengthen if more longitudinal PET-CT NSCLC data were available. Third, the stability of the features was examined on an external CT test-retest data set. Although two PET scans from patients within a short time interval are not commonly available, it is necessary to investigate the PET features reproducibility on such data set. Finally, the size of the patient material is admittedly rather small. Therefore, the capability of the proposed SALoP feature set for describing the intra-tumor heterogeneity should be investigated in future studies, including larger numbers of patients as well as other types of cancers.

5. Conclusions

This study investigated the early survival prediction of NSCLC in repeated PET-CT images by further developing a novel, easily interpretable, quantitative feature set which was capable of describing intra-tumor heterogeneity. Stability of the proposed feature set was validated on an external test-retest data set. Comparing the prognostic results of the proposed features with the radiomic approach, the prediction power of proposed feature set makes it promising as an imaging biomarker.

Acknowledgment

This study was supported by the Swedish Childhood Cancer Foundation (grant no. MT2016-0016) and the Swedish innovation agency Vinnova (grant no. 2017-01247). Additional funding from the Cancer Research Funds of Radiumhemmet is also acknowledged. Prof Philippe Lambin and Dr Wouter van Elmpt from Maastricht University Medical Center are kindly acknowledged for providing the patient data set used in this study. Initial data processing and support to data collection were supported by EU FP7 funding ARTFORCE.

Appendix A. Supplementary data

Supplementary data to this article can be found online at https://doi.org/10.1016/j.ejmp.2019.03.024.

References

[1] Torre LA, Bray F, Siegel RL, Ferlay J, Lortet-tieulent J, Jemal A. Global Cancer Statistics, 2012. CA Cancer J Clin 2015;65:87–108. https://doi.org/10.3322/caac.21262.
[2] Cancer Fact Sheet. World Heal Organ. http://www.who.int/mediacentre/factsheets/fs297/en/.
[3] Coroller TP, Grossmann P, Hou Y, Rios Velazquez E, Leijenaar RTH, Hermann G, et al. CT-based radiomic signature predicts distant metastasis in lung adenocarcinoma. Radiother Oncol 2015;114:345–50. https://doi.org/10.1016/j.radonc.2015.02.015.
[4] Fried DV, Tucker SL, Zhou S, Liao Z, Mawlawi O, Ibbott G, et al. Prognostic value and reproducibility of pretreatment ct texture features in stage III non-small cell lung cancer. Int J Radiat Oncol Biol Phys 2014;90:834–42. https://doi.org/10.1016/j.ijrobp.2014.07.020.
[5] Balagurunathan Y, Kumar V, Gu Y, Kim J, Wang H, Liu Y, et al. Test-retest reproducibility analysis of lung CT image features. J Digit Imaging 2014;27:805–23. https://doi.org/10.1007/s10278-014-9716-x.
[6] Lu W, Chen W. Positron emission tomography/computerized tomography for tumor response assessment—a review of clinical practices and radiomics studies. Transl Cancer Res 2016;5:364–70. https://doi.org/10.21037/tcr.2016.07.12.
[7] Wahl RL, Jacene H, Kasamon Y, Lodge MA. From RECIST to PERCIST: evolving considerations for PET response criteria in solid tumors. J Nucl Med 2009;50:122S–50S. https://doi.org/10.2967/jnumed.108.057307.
[8] Lee G, Lee HY, Park H, Schiebler ML, van Beek EJR, Ohno Y, et al. Radiomics and its emerging role in lung cancer research, imaging biomarkers and clinical management: state of the art. Eur J Radiol 2017;86:297–307. https://doi.org/10.1016/j.ejrad.2016.09.005.
[9] Lordick F, Ott K, Krause BJ, Weber WA, Becker K, Stein HJ, et al. PET to assess early metabolic response and to guide treatment of adenocarcinoma of the oesophagogastric junction: the MUNICON phase II trial. Lancet Oncol 2007;8:797–805. https://doi.org/10.1016/S1470-2045(07)70244-9.
[10] Kinahan PE, Fletcher JW. Positron emission tomography-computed tomography standardized uptake values in clinical practice and assessing response to therapy. Semin Ultrasound, CT MRI 2010;31:496–505. https://doi.org/10.1053/j.sult.2010.10.001.
[11] Zhao B, Tan Y, Tsai WY, Qi J, Xie C, Lu L, et al. Reproducibility of radiomics for deciphering tumor phenotype with imaging. Sci Rep 2016;6:1–7. https://doi.org/10.1038/srep23428.
[12] Zhang B, He X, Ouyang F, Gu D, Dong Y, Zhang L, et al. Radiomic machine-learning classifiers for prognostic biomarkers of advanced nasopharyngeal carcinoma. Cancer Lett 2017;403:21–7. https://doi.org/10.1016/j.canlet.2017.06.004.
[13] Pota M, Scalco E, Sanguineti G, Farneti A, Cattaneo GM, Rizzo G, et al. Early prediction of radiotherapy-induced parotid shrinkage and toxicity based on CT radiomics and fuzzy classification. Artif Intell Med 2017;81:41–53. https://doi.org/10.1016/j.artmed.2017.03.004.
[14] Moran A, Daly ME, Yip SSF, Yamamoto T. Radiomics-based assessment of radiation-induced lung injury after stereotactic body radiotherapy. Clin Lung Cancer 2017;18:e425–31. https://doi.org/10.1016/j.cllc.2017.05.014.
[15] Ou D, Blanchard P, Rosellini S, Levy A, Nguyen F, Leijenaar RTH, et al. Predictive and prognostic value of CT based radiomics signature in locally advanced head and neck cancers patients treated with concurrent chemoradiotherapy or bioradiotherapy and its added value to Human Papillomavirus status. Oral Oncol 2017;71:150–5. https://doi.org/10.1016/j.oraloncology.2017.06.015.
[16] Gillies RJ, Kinahan PE, Hricak H. Radiomics: images are more than pictures, they are data. Radiology 2016;278:563–77. https://doi.org/10.1148/radiol.2015151169.
[17] Aerts HJWL, Velazquez ER, Leijenaar RTH, Parmar C, Grossmann P, Cavalho S, et al. Decoding tumour phenotype by noninvasive imaging using a quantitative radiomics approach. Nat Commun 2014;5. https://doi.org/10.1038/ncomms5006.
[18] Lambin P, Rios-Velazquez E, Leijenaar R, Carvalho S, Van Stiphout RGPM, Granton P, et al. Radiomics: extracting more information from medical images using advanced feature analysis. Eur J Cancer 2012;48:441–6. https://doi.org/10.1016/j.ejca.2011.11.036.
[19] Larue RTHM, Van De Voorde L, van Timmeren JE, Leijenaar RTH, Berbée M, Sosef MN, et al. 4DCT imaging to assess radiomics feature stability: an investigation for thoracic cancers. Radiother Oncol 2017;125:147–53. https://doi.org/10.1016/j.radonc.2017.07.023.
[20] Lambin P, Leijenaar RTH, Deist TM, Peerlings J, de Jong EEC, van Timmeren J, et al. Radiomics: the bridge between medical imaging and personalized medicine. Nat Rev Clin Oncol 2017;14:749–62. https://doi.org/10.1038/nrclinonc.2017.141.
[21] Huynh E, Coroller TP, Narayan V, Agrawal V, Hou Y, Romano J, et al. CT-based radiomic analysis of stereotactic body radiation therapy patients with lung cancer. Radiother Oncol 2016;120:258–66. https://doi.org/10.1016/j.radonc.2016.05.024.
[22] van Timmeren JE, Leijenaar RTH, van Elmpt W, Reymen B, Oberije C, Monshouwer

R, et al. Survival prediction of non-small cell lung cancer patients using radiomics analyses of cone-beam CT images. Radiother Oncol 2017;123:363–9. https://doi.org/10.1016/j.radonc.2017.04.016.
[23] Coroller TP, Agrawal V, Narayan V, Hou Y, Grossmann P, Lee SW, et al. Radiomic phenotype features predict pathological response in non-small cell lung cancer. Radiother Oncol 2016;119:480–6. https://doi.org/10.1016/j.radonc.2016.04.004.
[24] Emaminejad N, Qian W, Guan Y, Tan M, Qiu Y, Liu H, et al. Fusion of quantitative image and genomic biomarkers to improve prognosis assessment of early stage lung cancer patients. IEEE Trans Biomed Eng 2016;63:1034–43. https://doi.org/10.1109/TBME.2015.2477688.
[25] Leijenaar RTH, Carvalho S, Velazquez ER, Van Elmpt WJC, Parmar C, Hoekstra OS, et al. Stability of FDG-PET radiomics features: an integrated analysis of test-retest and inter-observer variability. Acta Oncol (Madr) 2013;52:1391–7. https://doi.org/10.3109/0284186X.2013.812798.
[26] Huyge V, Garcia C, Alexiou J, Ameye L, Vanderlinden B, Lemort M, et al. Heterogeneity of metabolic response to systemic therapy in metastatic breast cancer patients. Clin Oncol 2010;22:818–27. https://doi.org/10.1016/j.clon.2010.05.021.
[27] O'Connor JPB, Rose CJ, Waterton JC, Carano RAD, Parker GJM, Jackson A. Imaging intratumor heterogeneity: Role in therapy response, resistance, and clinical outcome. Clin Cancer Res 2015;21:249–57. https://doi.org/10.1158/1078-0432.CCR-14-0990.
[28] Wu J, Gensheimer M, Dong X, Rubin D, Napel S, Diehn M, et al. Robust intratumor partitioning to identify high-risk subregions in lung cancer: a pilot study. Int J Radiat Oncol Biol Phys 2016;95:1504–12. https://doi.org/10.1016/j.ijrobp.2016.03.018.
[29] Buizza G, Toma-Dasu I, Lazzeroni M, Paganelli C, Riboldi M, Chang Y, et al. Early tumor response prediction for lung cancer patients using novel longitudinal pattern features from sequential PET/CT image scans. Phys Medica 2018;54:21–9. https://doi.org/10.1016/j.ejmp.2018.09.003.
[30] International Commission on Radiation Units: Prescribing, Recording, and Reporting Photon Beam Therapy. Washington, DC, 1993. doi: 10.2307/3578862.
[31] Nijsten SMJJG, Mijnheer BJ, Dekker ALAJ, Lambin P, Minken AWH. Routine individualised patient dosimetry using electronic portal imaging devices. Radiother Oncol 2007;83:65–75. https://doi.org/10.1016/j.radonc.2007.03.003.
[32] van Elmpt W, Ollers M, Dingemans A-MC, Lambin P, De Ruysscher D. Response assessment using 18F-FDG PET early in the course of radiotherapy correlates with survival in advanced-stage non-small cell lung cancer. J Nucl Med 2012;53:1514–20. https://doi.org/10.2967/jnumed.111.102566.
[33] Avanzo M, Stancanello J, El Naqa I. Beyond imaging: the promise of radiomics. Phys Medica 2017;38:122–39. https://doi.org/10.1016/j.ejmp.2017.05.071.
[34] Wang C, Frimmel H, Smedby Ö. Fast level-set based image segmentation using coherent propagation. Med Phys 2014;41:073501https://doi.org/10.1118/1.4881315.
[35] Wang C. Mia Lite Solution. http://www.mia-solution.com/products.html.
[36] Medical Image Processing and Visualization. https://www.mevislab.de/.
[37] Insight Segmentation and Registration Toolkit (ITK). https://itk.org/.
[38] Clark K, Vendt B, Smith K, Freymann J, Kirby J, Koppel P, et al. The cancer imaging archive (TCIA): maintaining and operating a public information repository. J Digit Imaging 2013;26:1045–57. https://doi.org/10.1007/s10278-013-9622-7.
[39] Zhao B, James LP, Moskowitz CS, Guo P, Ginsberg MS, Lefkowitz RA, et al. Evaluating variability in tumor measurements from same-day repeat CT scans of patients with non-small cell lung cancer. Radiology 2009;252:263–72. https://doi.org/10.1148/radiol.2522081593.
[40] Zhao B, James LP, Moskowitz CS, Guo P, Ginsberg MS. Data From RIDER_Lung CT. Cancer Imaging Arch.https://wiki.cancerimagingarchive.net/display/Public/RIDER+Lung+CT#b2e97b8e89914ca5acf418cd47bb7386.
[41] Zwanenburg A, Leger S, Vallières M, Löck S, Initiative for the IBS. Image biomarker standardisation initiative 2016. arXiv: 1612.07003.
[42] Vallières M, Freeman CR, Skamene SR, El Naqa I. A radiomics model from joint FDG-PET and MRI texture features for the prediction of lung metastases in soft-tissue sarcomas of the extremities. Phys Med Biol 2015;60:5471–96. https://doi.org/10.1088/0031-9155/60/14/5471.
[43] Toma-Dasu I, Uhrdin J, Lazzeroni M, Carvalho S, van Elmpt W, Lambin P, et al. Evaluating tumor response of non-small cell lung cancer patients with 18F-fludeoxyglucose positron emission tomography: potential for treatment individualization. Int J Radiat Oncol 2015;91:376–84. https://doi.org/10.1016/j.ijrobp.2014.10.012.
[44] Lin LI. A Concordance Correlation Coefficient to Evaluate Reproducibility Published by : International Biometric Society Stable URL : http://www.jstor.org/stable/2532051. 1989;45:255–68.
[45] Pudil P, Novovičová J, Kittler J. Floating search methods in feature selection. Pattern Recognit Lett 1994;15:1119–25. https://doi.org/10.1016/0167-8655(94)90127-9.
[46] Lian C, Ruan S, Denœux T, Jardin F, Vera P. Selecting radiomic features from FDG-PET images for cancer treatment outcome prediction. Med Image Anal 2016;32:257–68. https://doi.org/10.1016/j.media.2016.05.007.
[47] Mi H, Petitjean C, Dubray B, Vera P, Ruan S. Robust feature selection to predict tumor treatment outcome. Artif Intell Med 2015;64:195–204. https://doi.org/10.1016/j.artmed.2015.07.002.
[48] Coroller TP, Agrawal V, Huynh E, Narayan V, Lee SW, Mak RH, et al. Radiomic-based pathological response prediction from primary tumors and lymph nodes in NSCLC. J Thorac Oncol 2017;12:467–76. https://doi.org/10.1016/j.jtho.2016.11.2226.
[49] Jiang B, Zhang X, Cn ZE, Cai T, Edu TH. Estimating the confidence interval for prediction errors of support vector machine classifiers. J Mach Learn Res 2008;9:521–40.
[50] Vallières M. MATLAB programming tools for radiomics analysis. https://github.com/mvallieres/radiomics.
[51] DeLong ER, DeLong DM, Clarke-Pearson DL. Comparing the areas under two or more correlated receiver operating characteristic curves: a nonparametric approach. Biometrics 1988;44:837. https://doi.org/10.2307/2531595.
[52] Carvalho S, Leijenaar RTH, Troost EGC, van Elmpt W, Muratet J-P, Denis F, et al. Early variation of FDG-PET radiomics features in NSCLC is related to overall survival – the "delta radiomics" concept. Radiother Oncol 2016;118:S20–1. https://doi.org/10.1016/S0167-8140(16)30042-1.
[53] Huang Yanqi, Liu Zaiyi, He Lan, et al. Radiomics signature: a potential biomarker for the prediction of disease-free survival in early-stage (I or II) non—small cell lung cancer. Radiology 2016;281. https://doi.org/10.1148/radiol.2016152234.
[54] de Jong EEC, van Elmpt W, Rizzo S, Colarieti A, Spitaleri G, Leijenaar RTH, et al. Applicability of a prognostic CT-based radiomic signature model trained on stage I-III non-small cell lung cancer in stage IV non-small cell lung cancer. Lung Cancer 2018;124:6–11. https://doi.org/10.1016/j.lungcan.2018.07.023.
[55] Kirienko M, Cozzi L, Antunovic L, Lozza L, Fogliata A, Voulaz E, et al. Prediction of disease-free survival by the PET/CT radiomic signature in non-small cell lung cancer patients undergoing surgery. Eur J Nucl Med Mol Imaging 2018;45:207–17. https://doi.org/10.1007/s00259-017-3837-7.
[56] Carvalho S, Leijenaar RTH, Troost EGC, van Timmeren JE, Oberije C, van Elmpt W, et al. 18F-fluorodeoxyglucose positron-emission tomography (FDG-PET)-Radiomics of metastatic lymph nodes and primary tumor in non-small cell lung cancer (NSCLC) – a prospective externally validated study. PLoS ONE 2018;13:e0192859https://doi.org/10.1371/journal.pone.0192859.
[57] Jensen GL, Yost CM, Mackin DS, Fried DV, Zhou S, Court LE, et al. Prognostic value of combining a quantitative image feature from positron emission tomography with clinical factors in oligometastatic non-small cell lung cancer. Radiother Oncol 2018;126:362–7. https://doi.org/10.1016/j.radonc.2017.11.006.
[58] Fried David V, Tucker Susan L, Zhou Shouhao, Liao Zhongxing, Mawlawi Osama, Ibbott Geoffrey, et al. Prognostic value and reproducibility of pretreatment CT texture features in stage III non-small cell lung cancer. Int J Radiat Oncol Biol Physicsy Biol Phys 2014;9:834–42. https://doi.org/10.1016/j.ijrobp.2014.07.020.
[59] Dong Xinzhe, Sun Xiaorong, Sun Lu, Maxim Peter G, Xing Lei, Huang Yong, et al. Early change in metabolic tumor heterogeneity during chemoradiotherapy and its prognostic value for patients with locally advanced non-small cell lung cancer. PLoS ONE 2016;11. https://doi.org/10.1371/journal.pone.0157836.
[60] Cook Gary JR, O'Brien Mary E, Siddique Muhammad, Chicklore Sugama, Loi Hoi Y, Sharma Bhupinder, et al. Non-small cell lung cancer treated with erlotinib: heterogeneity of 18F-FDG uptake at PET—association with treatment response and prognosis. Radiology 2015;276:883–93. https://doi.org/10.1148/radiol.2015141309.
[61] Hatt M, Tixier F, Pierce L, Kinahan PE, Le Rest CC, Visvikis D. Characterization of PET/CT images using texture analysis: the past, the present… any future? Eur J Nucl Med Mol Imaging 2017;44:151–65. https://doi.org/10.1007/s00259-016-3427-0.
[62] Ganeshan B, Panayiotou E, Burnand K, Dizdarevic S, Miles K. Tumour heterogeneity in non-small cell lung carcinoma assessed by CT texture analysis: a potential marker of survival. Eur Radiol 2012;22:796–802. https://doi.org/10.1007/s00330-011-2319-8.